Zhou et al. *NPG Asia Materials* (2020)12:69
https://doi.org/10.1038/s41427-020-00250-3

NPG Asia Materials

ARTICLE Open Access

High-temperature ferromagnetic semiconductor with a field-tunable green fluorescent effect

Bowen Zhou[1,2], Qing Zhao[1], Zhehong Liu[1,2], Xudong Shen[1,2], Xubin Ye[1,2], Jiangjian Shi[1,2], Zhiyu Liao[1,2], Weipeng Wang[1,2], Zhiwei Hu[3], Hong-Ji Lin[4], Chien-Te Chen[4], Yuecheng Bian[5], Zhigao Sheng[5], Richeng Yu[1,2], Xianggang Qiu[1,2], Qingbo Meng[1,2], Zhi Li[6] and Youwen Long[1,2,7]

Abstract

Ferromagnetic semiconductors with luminescent effects provide a unique platform for studying magneto-electric-optical multifunctional devices. However, little is known about such materials with spin ordering well above room temperature. By using a unique high-pressure annealing method, a Cr and Fe disordered perovskite oxide $SrCr_{0.5}Fe_{0.5}O_{2.875}$ (SCFO) with a simple cubic structure was prepared. Magnetic measurements demonstrated the ferromagnetic behavior with a spin ordering temperature as high as 600 K. In contrast to metallic $SrCrO_3$ and $SrFeO_3$, SCFO, with a moderate oxygen deficiency, is a direct bandgap semiconductor with an energy gap of 2.28 eV, which is within the visible light region. As a consequence, SCFO displays a green fluorescent effect arising from the d–p bonding and anti-bonding states. Moreover, the photoluminescence intensity can be tuned by a magnetic field. This work opens up a new avenue for research on room-temperature multifunctional materials with coupled magnetic, electrical, and optical performance.

Introduction

Magnetic semiconductors display intriguing magneto-electric and magneto-optical properties, providing promising candidates for high-performance multifunctional spintronic devices such as spin field-effect transistors and magnetic random access memory devices[1–6]. For practical applications, a high spin ordering temperature (T_C) above room temperature (RT) is desirable. However, despite tremendous efforts, most reported intrinsic ferromagnetic (FM) semiconductors without element substitution and doped diluted magnetic semiconductors have low critical temperatures[7–12]. Recently, a few insulating/semiconducting two-dimensional van der Waals crystals, such as $Cr_2Ge_2Te_6$ and CrI_3, have been found to show ferromagnetism[13–15], but the T_C values are rather low. At present, the discovered FM compounds have rarely been known to show luminescence. Therefore, there is a pressing need to search luminescent ferromagnetic materials with spin ordering above RT for magneto-electric-optical coupled applications.

The bandgaps of transition-metal perovskite oxides are usually developed with the formation of charge or spin density wave states. However, both $SrCrO_3$ and $SrFeO_3$ perovskites are metallic because of a small hole-type Fermi pocket around some high symmetry points of the Brillouin zone[16–18]. These two compounds may be converted into semiconductors if the small hole-type Fermi pocket is removed, i.e., by removing some electrons and its dominating bands around the Fermi level. Since the bands intercepting the Fermi level are dominated by the O-2*p* orbitals, we can remove some O atoms to tune the electron transport. Thus, by delicate control of O vacancies in $SrCrO_3$ and $SrFeO_3$, the Fermi level can fall into the gap, leading to semiconducting/insulating behavior. On the other hand, the bandgap is tunable by transition metal doping, which can increase or decrease the local

Correspondence: Zhi Li (zhili@njust.edu.cn) or Youwen Long (ywlong@iphy.ac.cn)
[1]Beijing National Laboratory for Condensed Matter Physics, Institute of Physics, Chinese Academy of Sciences, Beijing 100190, China
[2]School of Physical Sciences, University of Chinese Academy of Sciences, Beijing 100049, China
Full list of author information is available at the end of the article

spin moment and therefore modify the magnetism. By decreasing the oxygen content and mixing Cr and Fe magnetic ions, an oxygen-deficient perovskite oxide $SrCr_{0.5}Fe_{0.5}O_{2.875}$ with a B-site disordered Cr/Fe distribution was designed and prepared under high-pressure and high-temperature conditions. Although the oxygen-rich $SrCrO_3$[19–23] and $SrFeO_3$[24–27] are AFM metals with lower ordering temperatures (<140 K), the oxygen-deficient SCFO was confirmed to be a high-temperature ($T_C \sim 600$ K) ferromagnetic semiconductor with a direct bandgap of 2.28 eV. Moreover, a green fluorescent effect, which is tunable by a magnetic field, was found to occur. These joint features make SCFO a rare material system to design multifunctional magneto-electric-optical coupling devices with promising applications at or even above RT.

Experimental section

Polycrystalline SCFO was prepared by a solid-state reaction under high-pressure and high-temperature conditions. The highly pure (>99.9 %) reactants SrO, Fe_2O_3, CrO_2, and CrO_3 were mixed at a ratio of 8:2:3:1. The finely mixed reactants were treated at 6 GPa and 1173 K for 30 min on a cubic anvil-type high-pressure apparatus. The phase quality of SCFO was characterized by powder X-ray diffraction (XRD) using a Huber diffractometer with Cu $K\alpha_1$ radiation at RT. Rietveld refinement of the XRD data was performed using the FullProf program[28]. High-resolution selected area electron diffraction was performed along the $[1-10]$ zone axis on an ARM200Fcold field emission transmission electron microscope. X-ray absorption spectroscopy at the Cr– and Fe–$L_{2,3}$ edges was performed at the BL11A beamline of the NSRRC synchrotron using total electron yield mode. The magnetic susceptibility and magnetization measurements were carried out using a superconducting quantum interference device magnetometer (Quantum Design, MPMS-VSM). The resistivity and specific heat were measured on a physical property measurement system (Quantum Design, PPMS-9T). We measured the visible and UV range frequency-dependent reflectivity from the surface at a near-normal angle of incidence on an Avaspec 2048 × 14 optical fiber spectrometer. The extinction coefficient was obtained through a Kramers-Kronig transformation of reflectivity at a near-normal angle of incidence in the range of 50–50,000 cm^{-1} on a Bruker 80v Fourier transform infrared spectrometer using an in situ evaporation technique. Steady-state photoluminescence measurements without a magnetic field were performed on an Edinburgh FLS 920 spectrometer by directing the excitation laser pulses of the pump fluence of ~0.5 nJ cm^{-2} at 445 nm. For the magnetic field-dependent photoluminescence spectra, the magnetic field was provided by a superconducting magnet, and the excitation light source was changed to HeCd lasers with a 325 nm wavelength (Kimmon Koha).

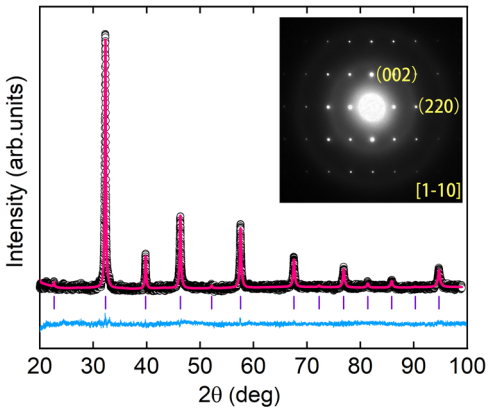

Fig. 1 XRD pattern and structure refinement results of SCFO obtained at RT. The observed (black circles), calculated (red line), and difference (blue line) are shown. The ticks indicate the allowed Bragg reflections with space group *Pm*-3*m*. The inset shows the selected area electron diffraction pattern along the [1 − 10] zone axis.

Results and discussion

Figure 1 shows the powder XRD pattern and the refinement results of SCFO synthesized at 6 GPa and 1173 K. All the diffraction peaks can be well fitted on the basis of a simple cubic perovskite structure with space group *Pm*-3*m*. The goodness of fit parameter was within a satisfactory range, with $R_{wp} = 2.01\%$. Moreover, high-resolution electron diffraction was performed along the [1-10] direction. One cannot discern any diffraction spots with $h + k + l =$ odd like (111) spot (see the inset of Fig. 1), further revealing the disordered distribution for Cr and Fe at the B site. Therefore, $SrCr_{0.5}Fe_{0.5}O_{2.875}$ possesses a crystal structure similar to that of undoped $SrCrO_3$[29] and $SrFeO_3$[30]. In comparison, the refined lattice constant of SCFO (3.9185 Å) is slightly larger than that of the oxygen-rich $SrCrO_3$ (3.818 Å) and $SrFeO_3$ (3.836 Å), which can be attributed to the oxygen deficiency in SCFO. To verify the valence states of Fe and Cr, element-sensitive soft X-ray absorption spectroscopy (XAS) was performed (see Supporting information Fig. S1)[31–35]. The XAS results show the charge combination in $SrCr^{4.5+}_{0.5}Fe^{3+}_{0.5}O_{2.875}$, where the average $Cr^{4.5+}$ is a mixture of Cr^{4+} and Cr^{6+} at a ratio of 3:1, revealing the occurrence of moderate oxygen deficiency. This charge combination is consistent with the nominal oxygen content during sample synthesis under high pressure ($8SrO + 2Fe_2O_3 + 3CrO_2 + CrO_3 = 8SrCr_{0.5}Fe_{0.5}O_{2.875}$). Note that in addition to controlling the oxygen content, high pressure is also necessary to stabilize the cubic perovskite structure of SCFO, similar to the high-pressure synthesis of isostructural $SrFeO_3$ and $SrCrO_3$.

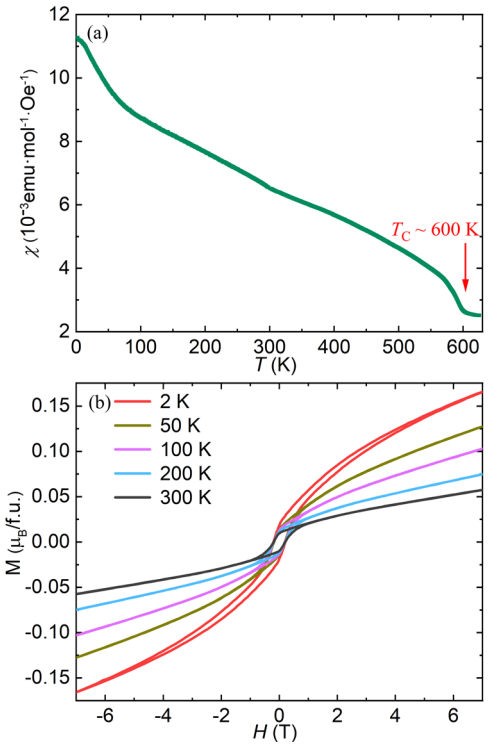

Fig. 2 Magnetic properties of SCFO. a Temperature dependence of the magnetic susceptibility measured at 0.1 T. **b** Isothermal magnetic hysteresis loops measured at different temperatures.

Figure 2a shows the temperature dependence of the magnetic susceptibility of SCFO measured under a magnetic field of $H = 0.1$ T using zero-field-cooling mode. Upon cooling to $T_C \sim 600$ K, the susceptibility experiences a sharp increase, suggesting an FM-like phase transition. Upon further cooling, the susceptibility smoothly increases, accompanied by an apparent upturn below approximately 80 K. If one looks at the field-dependent magnetization, as shown in Fig. 2b, remarkable magnetic hysteresis exists below T_C. At 300 K, the coercive field is approximately 2000 Oe, which is almost temperature independent upon cooling to 2 K. The remnant magnetization measured at 300 K is approximately 0.01 μ_B/f.u. and increases to 0.02 μ_B/f.u. at 2 K. These features indicate the canted ferromagnetism of SCFO, as reported in the ferroelectric ferromagnets of $BiFe_{1-x}Co_xO_3$ thin films and 1D $SrFeO_{2.5}$ chains[36,37]. In comparison, all of these FM compounds show similar magnitudes in remnant magnetization, but the coercive fields observed in SCFO and $BiFe_{1-x}Co_xO_3$ thin films are much higher than that of the $SrFeO_{2.5}$ chain (130 Oe). In SCFO, magnetic Fe^{3+} and Cr^{4+} ions exist at a ratio of 4:3. Since the *d*-electron amount of Fe^{3+} ($3d^5$) is considerably larger than that of Cr^{4+} ($3d^2$), the Fe^{3+}–O–Fe^{3+} superexchange interactions are expected to dominate the magnetism. The canted spins of Fe^{3+} ions are thus responsible for the high-temperature FM behavior of SCFO. In addition, the lower-temperature upturn observed in magnetic susceptibility below ~80 K is probably indicative of some short-range FM correlations due to the Fe^{3+}–O–Cr^{4+} superexchange interactions.

In comparison with the oxygen-rich perovskite oxides, i.e., the *C*-type AFM $SrCrO_3$ and spiral $SrFeO_3$ with lower Néel temperatures, Cr/Fe disordered SCFO with oxygen deficiency exhibits different magnetic features, with a high T_C well above RT. Moreover, unlike the metallic electrical transport properties observed in $SrCrO_3$ and $SrFeO_3$, the current SCFO displays semiconducting behavior, as evidenced by the sharply increased resistivity upon cooling (see Fig. S2). The resistivity data between 210 and 380 K follow a 3D Mott variable-range hopping model, as shown in the inset of Fig. S2 using the function $\rho = \rho_0 \exp(T_0/T)^{1/4}$, where ρ_0 is the prefactor and T_0 represents the characteristic temperature[38]. As shown in Fig. S3, the specific heat of SCFO does not display any anomalies from 2 to 200 K. At lower temperatures (<12 K), the data can be fitted using the function $C_p = \alpha T^{3/2} + \beta T^3$, yielding $\alpha = 8.3$ mJ/mol·K$^{5/2}$ and $\beta = 0.16$ mJ/mol·K^4. The presence of the $T^{3/2}$ term is in agreement with the FM behavior. The absence of an electron contribution to specific heat (proportional to T) suggests the semiconducting or insulating nature with a considerable bandgap in SCFO.

To investigate the detailed energy bandgap of SCFO, reflectance spectra in the UV-visible region were obtained at RT, as shown in Fig. 3a. Although the reflectivity for a polycrystalline sample is usually not as strong in the wavelength range from 400 to 800 nm, a sharp peak is found to occur at 545.5 nm in SCFO. Moreover, other smaller peaks are also observed, which can be attributed to the formation of some bound exciton states[39,40]. We obtained the absorption coefficient α_0 according to the equation $\alpha_0 = 4\pi\kappa/\lambda$, where the extinction coefficient κ was detected from 50 to 50,000 cm^{-1}. With the major optical transitions described, we used the Tauc and Davis-Mott models[41] based on the equation $\alpha_0 h\nu = A(h\nu - E_g)^n$, where A is a proportional constant, E_g is the optical bandgap and n depends on the type of band transition of the material. For materials with a direct (indirect) bandgap, $n = 1/2$ (2) is assigned. A direct bandgap of Tauc's plots exhibiting $(\alpha_0 h\nu)^2$ versus photon energy $h\nu$ has been revealed for SCFO, as shown in Fig. 3b, yielding a bandgap of $E_g = 2.28$ eV ($\lambda = 545.2$ nm), which is consistent with the strongest peak observed in the reflectance spectrum at 545.5 nm. The E_g of SCFO is close to the bandgaps of $LaFeO_3$ (~2.34 eV)[42] and $SrCrO_4$ (~2.45 eV)[43]. Note that

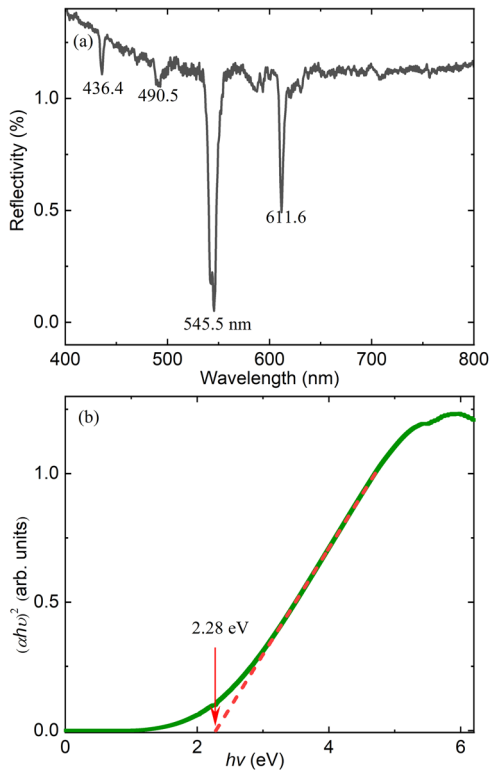

Fig. 3 Optical properties of SCFO. a Room-temperature UV-visible reflectance spectra. **b** Direct bandgap plots $(ahv)^2$ versus hv for SCFO. The direct-allowed transition model indicates E_g to be 2.28 eV.

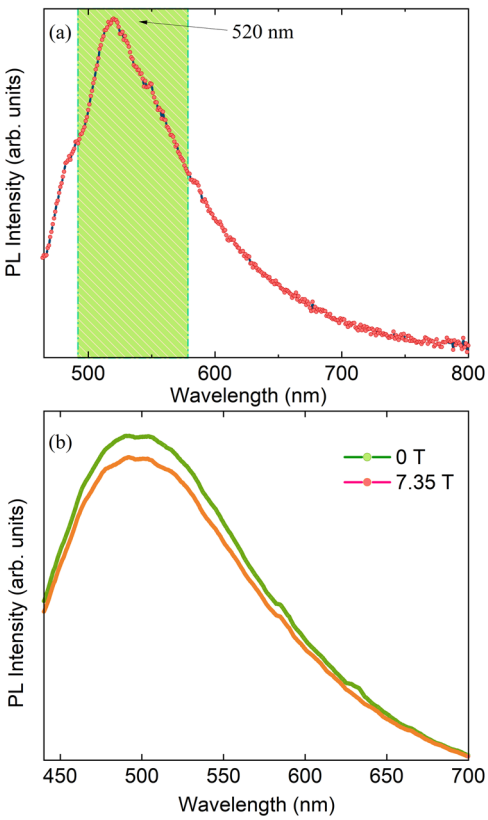

Fig. 4 Photoluminescent properties of SCFO. a Photoluminescence (PL) spectra measured at RT after photoexcitation by 445 nm blue light. The green rectangular area of the shadow shows the green light region. **b** Photoluminescence spectra of SCFO at zero field and 7.35 T using 325 nm excitation light.

the wavelength of the bandgap energy lies in the visible light range, particularly in the green wavelength region. The direct-gap nature of SCFO makes it possible to generate light emission.

Figure 4a shows the photoluminescence measurement result of SCFO. A broad green emission peak can be observed at approximately $\lambda = 520$ nm upon excitation by blue light at a wavelength of 445 nm. The peak energy is somewhat larger than E_g (~545 nm), suggesting that the green light emission mainly emanates from an across-bandgap (band-to-band) transition. There are some empty *d*-orbitals dominating the band between the *d*–*p* bonding and anti-bonding states. Therefore, except for the electronic transition between the *d*–*p* bonding and anti-bonding states, there are additional photoluminescence lines mediated by the empty and localized *d*-orbitals between the *d*–*p* bonding state and anti-bonding states, giving rise to photon energies larger than the bandgap. Moreover, the full width at half maximum completely covers the green light region (see the shaded part in Fig. 4a). This broadening effect may result from band-edge absorption and multiple exciton states, such as the charge trapping that exists in polycrystalline samples[44]. On the other hand, from the viewpoint of the electronic configuration, unlike the *f*–*f* transition emission spectra of rare earth ions[45] where *f* electrons are screened by outer 5*s* and 5*p* electrons so that the emission spectra peaks are sharp and more similar to atomic emission line spectra, *d* electronic transition emission spectra show peak broadening as a consequence of band broadening of the outer *d* electrons sensitive to the crystal field environment.

Since the transition-metal 3*d* electrons in SCFO take part in spin ordering, the related fluorescent effect can be tuned by an external magnetic field. Fig. 4b presents the photoluminescence spectra measured at zero field and 7.35 T using 325 nm excitation light. Apparently, applying a magnetic field can effectively change the luminescence intensity, suggesting the occurrence of magneto-optical coupling. Usually, fluorescent effects are observed in inorganic semiconductors with rare earth element activators or bound excitation states. The current SCFO provides a new photoluminescence system that is

composed of 3*d* transition metals rather than expensive rare earth elements. The empty *d*-orbitals separate the *d*–*p* bonding and anti-bonding states, which serve as *f*-orbitals from activators or exciton states. Moreover, the local spin moments of rare earth elements are paramagnetic at RT because of the weak exchange interactions between them, whereas the spin moments are ordered well above RT in SCFO, providing an excellent platform for research on the interaction between spin order and photoluminescence.

In conclusion, a magnetic semiconductor, SCFO, with a high T_C (~600 K) was synthesized, and its green photoluminescence was studied. The magnetism and electron transport properties of SCFO are also presented in this report. Oxygen-vacancy modulation by the high-pressure and high-temperature synthesis method controls the crystal structure, electronic configurations, magnetic interactions, and bandgap energy. A specific direct bandgap structure induces green light emission, which provides an additional important degree of freedom for designing bulk materials with ferromagnetic and semiconducting properties. Our results suggest that SCFO is an available candidate for multifunctional magneto-electric-optical coupling devices with potential applications above room temperature.

Acknowledgements
This work was supported by the National Key R&D Program of China (Grant Nos. 2018YFE0103200 and 2018YFA0305700), the National Natural Science Foundation of China (Grant Nos. 11934017, 51772324, 11921004, 11574378, and 11574316), and the Chinese Academy of Sciences (Grant Nos. XDB33010200 and QYZDB–SSW–SLH013). We acknowledge the support from the Max Planck-POSTECH-Hsinchu Center for Complex Phase Materials. A portion of this work was performed on the Steady High Magnetic Field Facilities, High Magnetic Field Laboratory, CAS.

Author details
[1]Beijing National Laboratory for Condensed Matter Physics, Institute of Physics, Chinese Academy of Sciences, Beijing 100190, China. [2]School of Physical Sciences, University of Chinese Academy of Sciences, Beijing 100049, China. [3]Max Planck Institute for Chemical Physics of Solids, Dresden 01187, Germany. [4]National Synchrotron Radiation Research Center, Hsinchu 30076, Taiwan. [5]Anhui Key Laboratory of Condensed Matter Physics at Extreme Conditions, High Magnetic Field Laboratory, Chinese Academy of Sciences, Hefei 230031, China. [6]School of Materials Science and Engineering, Nanjing University of Science and Technology, Nanjing 210094, China. [7]Songshan Lake Materials Laboratory, Dongguan, Guangdong 523808, China

Conflict of interest
The authors declare that they have no conflict of interest.

Supplementary information is available for this paper at https://doi.org/10.1038/s41427-020-00250-3.

Received: 26 May 2020 Revised: 13 August 2020 Accepted: 13 August 2020
Published online: 23 October 2020

References

1. Awschalom, D. D. & Flatté, M. E. Challenges for semiconductor spintronics. *Nat. Phys.* **3**, 153–159 (2007).
2. Furdyna, J. K. Diluted magnetic semiconductors. *J. Appl. Phys.* **64**, 29–64 (1988).
3. Celotta, R. J. & Pierce, D. T. Polarized electron probes of magnetic surfaces. *Science* **234**, 333 (1986).
4. Prellier, W., Fouchet, A. & Mercey, B. Oxide-diluted magnetic semiconductors: a review of the experimental status. *J. Phys.: Condens. Matter* **15**, 1583–1601 (2003).
5. Manser, J. S., Christians, J. A. & Kamat, P. V. Intriguing optoelectronic properties of metal halide perovskites. *Chem. Rev.* **116**, 12956–13008 (2016).
6. Efros, Al. L. & Rosen, M. The electronic structure of semiconductor nanocrystals. *Annu. Rev. Mater. Sci.* **30**, 475–521 (2000).
7. MacDonald, A. H., Schiffer, P. & Samarth, N. Ferromagnetic semiconductors: moving beyond (Ga,Mn)As. *Nat. Mater.* **4**, 195–202 (2005).
8. Nagaev, E. L. Colossal-magnetoresistance materials: manganites and conventional ferromagnetic semiconductors. *Phys. Rep.* **346**, 387–531 (2001).
9. Dietl, T. & Ohno, H. Dilute ferromagnetic semiconductors: physics and spintronic structures. *Rev. Mod. Phys.* **86**, 187–251 (2014).
10. Santos, T. S. & Moodera, J. S. Observation of spin filtering with a ferromagnetic EuO tunnel barrier. *Phys. Rev. B* **69**, 241203 (2004).
11. Dietl, T., Haury, A. & Merle dAubigné, Y. Free carrier-induced ferromagnetism in structures of diluted magnetic semiconductors. *Phys. Rev. B* **55**, 3347–3350 (1997).
12. Lüders, U. et al. Spin filtering through ferrimagnetic $NiFe_2O_4$ tunnel barriers. *Appl. Phys. Lett.* **88**, 082505 (2006).
13. Carteaux, V., Brunet, D., Ouvrard, G. & Andre, G. Crystallographic, magnetic and electronic structures of a new layered ferromagnetic compound $Cr_2Ge_2Te_6$. *J. Phys.: Condens. Matter* **7**, 69–87 (1995).
14. McGuire, M. A., Dixit, H., Cooper, V. R. & Sales, B. C. Coupling of crystal structure and magnetism in the layered, ferromagnetic insulator CrI_3. *Chem. Mater.* **27**, 612–620 (2015).
15. Huang, B. et al. Electrical control of 2D magnetism in bilayer CrI_3. *Nat. Nanotechnol.* **13**, 544–548 (2018).
16. Lee, K. W. & Pickett, W. E. Orbital-ordering driven structural distortion in metallic $SrCrO_3$. *Phys. Rev. B* **80**, 6 (2009).
17. Rached, H., Rached, D., Rabah, M., Khenata, R. & Reshak, A. H. Full-potential calculation of the structural, elastic, electronic and magnetic properties of $XFeO_3$ (X = Sr and Ba) perovskite. *Phys. B* **405**, 3515–3519 (2010).
18. Mathi Jaya, S., Jagadish, R., Rao, R. S. & Asokamani, R. Electronic structure and magnetism of $SrFeO_3$ and $SrCoO_3$. *Phys. Rev. B: Condens. Matter* **43**, 13274–13279 (1991).
19. MacChesney, J. B., Sherwood, R. C. & Potter, J. F. Electric and magnetic properties of the strontium ferrates. *J. Chem. Phys.* **43**, 1907–1913 (1965).
20. Takeda, T., Yamaguchi, Y. & Watanabe, H. Magnetic structure of $SrFeO_3$. *J. Phys. Soc. Jpn.* **33**, 967–969 (1972).
21. Li, Z., Laskowski, R., Iitaka, T. & Tohyama, T. First-principles calculation of helical spin order in iron perovskite $SrFeO_3$ and $BaFeO_3$. *Phys. Rev. B* **85**, 134419 (2012).
22. Mostovoy, M. Helicoidal ordering in iron perovskites. *Phys. Rev. Lett.* **94**, 137205 (2005).
23. Komarek, A. C. et al. Magnetic order, transport and infrared optical properties in the $ACrO_3$ system (A = Ca, Sr, and Pb). *Phys. Rev. B* **84**, 14 (2011).
24. Long, Y. et al. Crossover from itinerant-electron to localized-electron behavior in $Sr_{1-x}Ca_xCrO_3$ perovskite solid solution. *J. Phys.: Condens. Matter* **23**, 355601 (2011).
25. Ortega-San-Martin, L. et al. Microstrain sensitivity of orbital and electronic phase separation in $SrCrO_3$. *Phys. Rev. Lett.* **99**, 255701 (2007).
26. Qian, Y., Wang, G., Li, Z., Jin, C. Q. & Fang, Z. The electronic structure of a weakly correlated antiferromagnetic metal, $SrCrO_3$: first-principles calculations. *N. J. Phys.* **13**, 053002 (2011).
27. Zhou, J. S., Jin, C. Q., Long, Y. W., Yang, L. X. & Goodenough, J. B. Anomalous electronic state in $CaCrO_3$ and $SrCrO_3$. *Phys. Rev. Lett.* **96**, 4 (2006).
28. Rodríguez-Carvajal, J. Recent advances in magnetic structure determination by neutron powder diffraction. *Phys. B* **192**, 55–69 (1993).
29. Chamberland, B. L. Preparation and properties of $SrCrO_3$. *Solid State Commun.* **5**, 663–666 (1967).
30. Wattiaux, A. et al. A novel preparation method of the $SrFeO_3$ cubic perovskite by electrochemical means. *Solid State Commun.* **77**, 489–493 (1991).

31. Majdoub, M. S., Sharma, P. & Çağin, T. Erratum: Enhanced size-dependent piezoelectricity and elasticity in nanostructures due to the flexoelectric effect. *Phys. Rev. B* **79**, 119904 (2009).
32. Deng, H. et al. Strong enhancement of spin ordering by A-site magnetic ions in the ferrimagnet $CaCu_3Fe_2Os_2O_{12}$. *Phys. Rev. B* **94**, 024414 (2016).
33. Wu, M. et al. Pressure-induced valence change and semiconductor–metal transition in $PbCrO_3$. *J. Phys. Chem. C.* **118**, 23274–23278 (2014).
34. Wong, C. J. et al. Anionic ordering in $Ba_{15}V_{12}S_{34}O_3$, Affording three oxidation states of vanadium and a quasi-one-dimensional magnetic lattice. *Chem. Mater.* **28**, 1621–1624 (2016).
35. Tsuyama, T. et al. X-ray spectroscopic study of $BaFeO_3$ thin films: an Fe^{4+} ferromagnetic insulator. *Phys. Rev. B* **91**, 115101 (2015).
36. Hojo, H. et al. Ferromagnetism at room temperature induced by spin structure change in $BiFe_{1-x}Co_xO_3$ thin films. *Adv. Mater.* **29**, 1603131 (2017).
37. Kang, K. T. et al. A room-temperature ferroelectric ferromagnet in a 1D tetrahedral chain network. *Adv. Mater.* **31**, 1808104 (2019).
38. Mott, N. F. Conduction in non-crystalline materials. *Philos. Mag.* **19**, 835–852 (1969).
39. Friemel, G. et al. Resonant magnetic exciton mode in the heavy-fermion antiferromagnet CeB_6. *Nat. Commun.* **3**, 830 (2012).
40. Heiss, W., Prechtl, G. & Springholz, G. Giant tunability of exciton photoluminescence emission in antiferromagnetic EuTe. *Phys. Rev. B* **63**, 165323 (2001).
41. Ibrahim, A. & Al-Ani, S. K. J. Models of optical absorption in amorphous semiconductors at the absorption edge — a review and re-evaluation. *Czechoslov. J. Phys.* **44**, 785–797 (1994).
42. Scafetta, M. D., Cordi, A. M., Rondinelli, J. M. & May, S. J. Band structure and optical transitions in $LaFeO_3$: theory and experiment. *J. Phys.: Condens. Matter* **26**, 505502 (2014).
43. Errandonea, D. et al. Theoretical and experimental study of the crystal structures, lattice vibrations, and band structures of monazite-type $PbCrO_4$, $PbSeO_4$, $SrCrO_4$, and $SrSeO_4$. *Inorg. Chem.* **54**, 7524–7535 (2015).
44. Wu, B. et al. Discerning the surface and bulk recombination kinetics of organic-inorganic halide perovskite single crystals. *Adv. Energy Mater.* **6**, 1600551 (2016).
45. Bünzli, J.-C. G., Comby, S., Chauvin, A.-S. & Vandevyver, C. D. B. New opportunities for lanthanide luminescence. *J. Rare Earths* **25**, 257–274 (2007).